Unsteady Aerodynamics of Slender Delta Wings at Large Angles of Attack

L. E. Ericsson* and J. P. Reding†
Lockheed Missiles & Space Company, Inc., Sunnyvale, Calif.

An analysis of the steady and unsteady aerodynamics of sharp-edged slender wings has been performed. The results show that slender wing theory can be modified to give the potential flow static and dynamic characteristics in incompressible flow. A semiempirical approximation is developed for the vortex-induced loads, and it is shown that the analytic approximation for sharp-edged slender wings gives good prediction of experimentally determined steady and unsteady aerodynamics. The results indicate that the effects of delta planform lifting surfaces can be included in a simple manner when determining the aeroelastic characteristics of the space shuttle lift-off configuration.

Nomenclature

A = aspect ratio, $A = b^2/S$
A_{TE} = inefficient wing area at $M = 0$ (Fig. 1)
b = wing span
$\bar{c}$ = reference length (usually mean aerodynamic chord, for a delta wing $\bar{c} = 2c_0/3$)
c_0 = root chord
K_p, K_V = potential flow and vortex lift factors, Eq. (1)
K_1, K_2 = constants, Eqs. (10) and (11)
k_1 = constant for α-dependence of vortex strength, Eq. (12)
L = lift: coefficient $C_L = L/(\rho_\infty U_\infty^2/2)S$
M = Mach number
M_p = pitching moment: coefficient $C_m = M_p/(\rho_\infty U_\infty^2/2)S\bar{c}$
N = normal force: coefficient $C_N = N/(\rho_\infty U_\infty{}^2/2)S$
p = static pressure: coefficient $C_p = (p - p_\infty)/(\rho_\infty U_\infty{}^2/2)$
q = pitch rate
Re = Reynolds number based on c_0 and freestream conditions
S = reference area (= projected wing area)
s = local semispan
t = time
Δt = timelag
U = horizontal velocity
$\bar{U}$ = convection velocity
x = axial body-fixed coordinate (Fig. 1)
y = spanwise body-fixed coordinate (Fig. 1)
z = vertical body-fixed coordinate octogonal to the x-y plane
ζ = dimensionless z-coordinate, $\zeta = z/c_0$
α = angle of attack
α_0 = trim angle of attack
ϵ = vortex contribution to apparent mass, Eq. (8)
Γ = vortex strength
η = dimensionless y-coordinate, $\eta = y/s$
θ = angular perturbation in pitch
θ_c = cone half angle
θ_{LE} = apex half angle (Fig. 1)
Λ = leading edge sweep angle, $\Lambda = \pi/2 - \theta_{LE}$
ξ = dimensionless x-coordinate, $\xi = x/c_0$
ρ = air density
ϕ = phase angle
$\Delta\phi$ = phase lag
ω = rigid body frequency
$\bar{\omega}$ = reduced frequency, $\bar{\omega} = \omega c_0/U_\infty$

Subscripts

a = attached flow
CG = center of gravity
eff = effective
LE = leading edge
max = maximum
$\perp$ = normal to leading edge
n = harmonic component
s = separated flow
TE = trailing edge
V = vortex
∞ = freestream conditions

Superscripts

$(-)$ = barred quantities denote integrated man values, e.g., centroid of aerodynamic loads

Differential Symbols

$\dot{\theta}$ = $\partial\theta/\partial t$; $\ddot{\theta} = \partial^2\theta/\partial t^2$
$C_{L\alpha}$ = $\partial C_L/\partial\alpha$; $C_{M_\theta} = \partial C_m/\partial\theta$
$C_{m_{\dot{\theta}}}$ = $C_{mq} + C_{m\dot{\alpha}} = \partial C_m/\partial(\bar{c}\dot{\theta}U_\infty)$; $C_{mq} = \partial C_m/\partial(\bar{c}q/U_\infty)$

Submitted June 24, 1974; presented as Paper 74-817 at the AIAA Mechanics and Control of Flight Conference, Anaheim, California, August 5-9, 1974; revision received January 30, 1975. The paper is based upon results obtained in a study made for the NASA Marshall Space Flight Center, Contract NAS8-28130, under direction of W. W. Clever.

Index categories: Aircraft Aerodynamics, (including Component Aerodynamics); Aircraft Vibration.

*Consulting Engineer. Associate Fellow AIAA.
†Research Specialist. Member AIAA.

Introduction

IT was clear very early in the space shuttle development that the vehicle design could be critically dependent upon aeroelastic loads.[1,2] The NASA Marshall Space Flight Center needed, therefore, to develop analytic methods in time to be applicable to the final space shuttle design. The main problem was that the methods would to a great extent be configuration dependent, and the configuration was changing continually. However, once the large crossrange capability had been decided upon, one design feature has remained fixed; that is, the orbiter will have a delta wing planform of some sort. The NASA MSFC concluded, therefore, that analytic or other means would be needed for prediction of unsteady delta wing aerodynamics regardless of future configuration changes.

The complexity of the flowfield prohibits the prediction of unsteady aerodynamic loads by purely theoretical means. It is

also well known from the Saturn-Apollo design that one cannot rely solely on dynamic experiments either, as the long lead time needed for the elastic model design in combination with the continuing changes of the flight vehicle predestines the test results to be obsolete when finally obtained. Regardless of the accuracy of the test data, they are of no help unless they can be "extrapolated analytically" to apply to the current flight vehicle design. Lockheed developed such analytical means for the Saturn-Apollo launch vehicles[3] and the predictions agreed so well with the elastic wind tunnel test results for the Saturn I booster[4,5] that this technique was used to predict the aeroelastic characterisitcs of all future Saturn boosters,[6] eliminating the need for further complicated elastic model tests.[7]

Based upon this past experience, NASA MSFC asked Lockheed Missiles & Space Co. to investigate the unsteady aerodynamics of the delta planform space shuttle, and try to develop analytic methods simple enough to allow the inclusion of large planform lifting surfaces in the computation of the aeroelastic characteristics of the space shuttle ascent configuration. The present paper reports on the results obtained for the basic delta wing.[8]

Analytic Approach

The same analytic approach that was used to determine the aeroelastic characteristics of the Apollo-Saturn launch vehicles[3,4] is used also here in developing analytic means for computation of the unsteady delta wing aerodynamics. That is, the attached flow characteristics are determined using a modified slender wing (or slender body) theory, and the unsteady aerodynamic characteristics of leeside separated flow (leading-edge vortices) are superimposed using static experimental data to define the separation-induced load distribution.

Analysis

The simple flow concept developed by Polhamus, i.e., the "turned-around" leading-edge suction, has been remarkably successful in predicting the nonlinear lift generated by the leading-edge vortex on slender wings at high angles of attack.[9] This is true not only for simple delta wings, but also for so-called double-deltas, and the method also predicts experimentally observed Mach number effects.[10] As the vortex lift is in reality dependent upon upstream flow conditions, and the leading-edge suction depends only upon local conditions, the flow concept cannot be applied to the unsteady aerodynamics. However, it is a very useful tool for determination of the static loads and is used as a starting point in the present analysis.

Static Characteristics

Polhamus' expression for the delta wing lift is[9]

$$C_L = C_{L,P} + C_{L,V}$$

$$C_{L,P} = K_p \sin\alpha \cos^2\alpha$$

$$C_{L,V} = K_V \sin^2\alpha \cos\alpha \qquad (1)$$

K_P and K_V are constants determining the magnitudes of attached flow and vortex lift components, respectively. K_V is for all practical purposes a true constant[9,10] $K_V = \pi$, whereas K_P is more or less linearly dependent upon aspect ratio (Fig. 1). The deviation between Jones' slender wing theory[11] and Polhamus' incompressible flow results are represented as follows in what is called "Present First Approximation" in Fig. 1. It is assumed that the area denoted A_{TE} in the inset of the figure carries no load. This accounts in a crude manner for the delta wing trailing edge condition at $M=0$, reducing the slender wing lift by the factor $\cos^2\theta_{LE}$. The following expression for K_p results in

$$K_p = \pi(A/2) / [1 + (A/4)^2] \qquad (2)$$

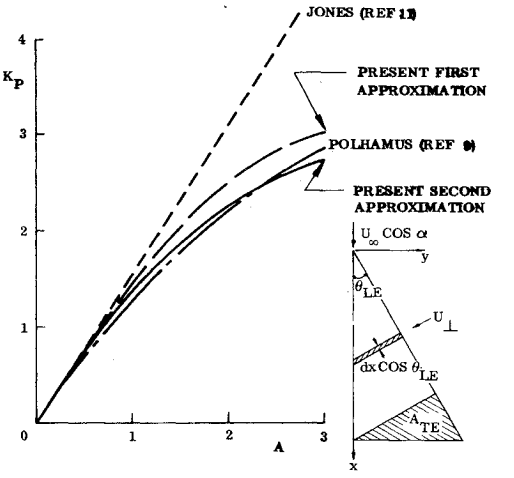

Fig. 1 Attached flow lift factor K_p of delta wings at $M=0$.

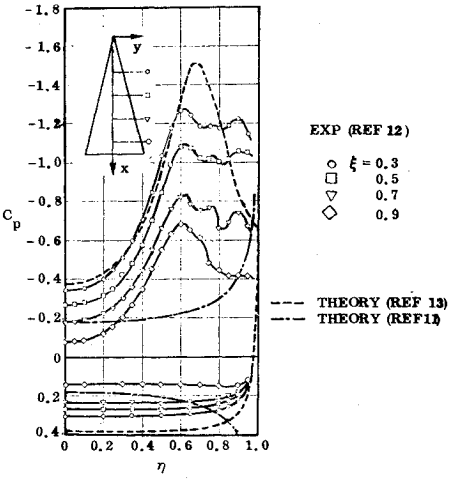

Fig. 2 Pressure distribution on an $A=1$ sharp-edged delta wing at $\alpha=20.5°$ and $M=0$.

This is the "First Approximation" shown in Fig. 1. At $M=1$ it is assumed that the area A_{TE} is fully effective, i.e., $K_p=\pi A/2$ in full agreement with Jones' theory.[11] The strip load normal to the leading edge (see insert in Fig. 1) is‡

$$(1/2)(d\,C_{Na}/d\xi)_\perp = [\pi \sin 2\alpha \sin^2\theta_{LE}/(b/2c_0)]\xi \qquad (3)$$

The conical flow assumption inherent in all existing theories does not seem to be substantiated by experimental results,[12] at least not for thin, sharp-edged delta wings (Fig. 2). Only close to the apex does the pressure distribution agree reasonably well with the best available theory.[13] Farther aft, the pressure level drops from the (constant) conical flow value, although the spanwise distribution remains very similar in shape. The deviation between theoretical and experimental spanwise load distributions is mainly due to secondary and tertiary flow separations that have much more prominent effects in a low Reynolds number wind-tunnel test than in actual high Reynolds number flight conditions.[12,14] In the flight case, the boundary layer over the center wing will not be laminar but turbulent, and the secondary separation and its effects will be much smaller. The fall-off from the conical flow level of the aft delta wing pressures (Fig. 2) indicates that far downstream from the apex the feeding sheet from the leading edge is changing, and the vortex strength farther aft is no longer growing linearly with ξ. The measured load distributions[15] on a sharp-edged $A=1.147$ delta wing at $\alpha=10°$, 20°, and 30° are shown in Fig. 3. Also shown is the attached flow slender

‡Note that $C_L = C_N \cos\infty$.

wing load distribution defined by Eq. (3). The measured load distribution is fairly well approximated by using a bilinear approximation to the nonlinear vortex-lift distribution, with the break occurring at $\xi = 0.4$.

The trailing-edge-round-off in the measured load distribution would be obtained, it appears, if the attached flow load distribution were represented by a more accurate potential flow lift distribution,[16,17] shown as a short-dash line in Fig. 3. Further comparison in this respect is made in Fig. 4, showing that limiting the attached flow lift growth in Eq. (3) to $(dC_N/d\xi)/C_N = 1.5$ gives better agreement with the distribution given by vortex-lattice methods.[16,17] It is obvious that the aspect ratio should not be much larger than $A = 2$ when applying the present modified slender wing distribution. Applying this "ceiling" to the lift growth decreases $C_{N\alpha}$ by 9%. This is the "present second approximation" for K_p shown in Fig. 1, which is in better agreement with Polhamus' potential flow value. With this modification, Eq. (3) becomes§

$$(1/2)\,(dC_{Na}/d\xi)_{\perp} = \frac{\pi \sin 2\alpha \sin^2\theta_{LE}}{(b/2c_0)} \times \begin{cases} \xi & : \xi \le 0.7 \\ 0.7 & : \xi > 0.7 \end{cases} \tag{4}$$

Integration gives

$$C_{Na} = 0.91\pi \sin 2\alpha \sin^2\theta_{LE}/(b/c_0) \tag{5a}$$

$$C_{ma} = -(c_0/\bar{c})C_{Na}(\bar{\xi}_a - \xi_{CG}) \tag{5b}$$

$$\bar{\xi}_a = 0.64(1 - \Delta\xi_{aTE}) \tag{5c}$$

$$\Delta\xi_{aTE} = \eta_a \sin^2\theta_{LE} \quad (\eta_a = 4/3\pi\text{:elliptic loading}) \tag{5d}$$

There is, of course, every reason to believe that the vortex-induced load distribution should have a trailing-edge-round-off effect similar to that for the attached flow loads. As a matter of fact, flow visualization results show the vortices to bend away into the freestream (some 10%) before the trailing edge.[18,19] To be consistent, the vortex-induced loads are assumed to have the same type of "triangular round-off" as the attached flow loads.

$$(1/2)\left[\frac{dC_{NV}}{d\xi}\right]_{\perp} = \begin{cases} 1.72\ \pi\xi\sin^2\alpha\text{:}\ \xi \le 0.4 \\ 6.85\pi\ \sin^2\alpha\text{:}\ 0.4 < \xi \le 1.0 \\ 6.85\pi\ \sin^2\alpha(1-\xi)\text{:}\ 0.9 \le \xi \le 1.0 \end{cases} \tag{6}$$

The integrated total vortex load for a delta wing is that given by Polhamus,[9,10] Eq. (1), with $K_V = \pi$. The capability of Polhamus' leading-edge suction analogy to predict the measured vortex-induced lift has been demonstrated.[9,10] Equation (6) only redistributes the lift to fit the experimentally observed lift distribution. After integration, Eq. (6) gives the following loads

$$C_{NV} = \pi \sin^2\alpha \tag{7a}$$

$$C_{mV} = -(c_0/\bar{c})C_{NV}(\bar{\xi}_V - \xi_{CG}) \tag{7b}$$

$$\bar{\xi}_V = 0.56(1 - \Delta\xi_{VTE}) \tag{7c}$$

$$\Delta\xi_{VTE} = \bar{\eta}_V \sin^2\theta_{LE} \quad (\bar{\eta}_V \approx 0.75) \tag{7d}$$

Figure 5 shows that although the experimental $C_m(\alpha)$ – characteristics are predicted better by Eqs. (5) and (7) than by the strict application of the leading-edge- suction analogy,[10,20] the prediction is not as good as one would expect in view of the fact that experimental data were used to define the

§With the strip still normal to the leading edge, as defined in the inset in Fig. 1.

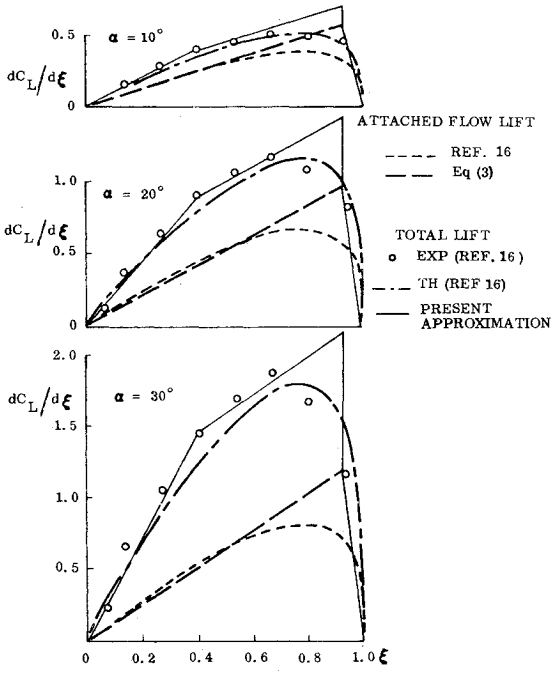

Fig. 3 Lift distribution components on an $A = 1.147$ delta wing.

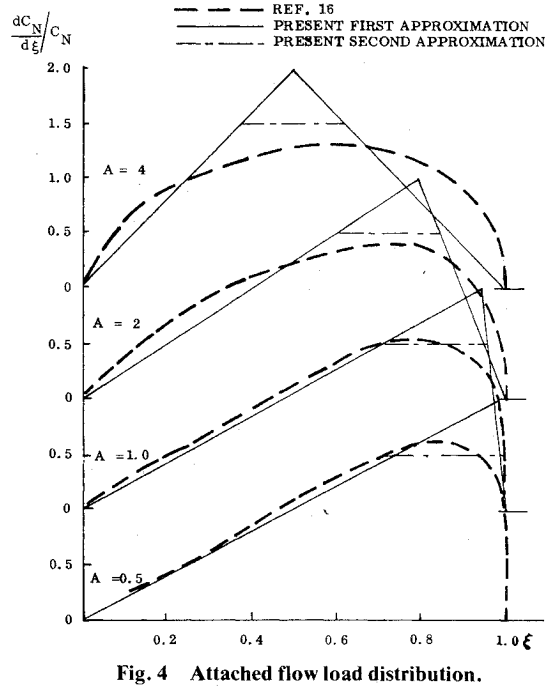

Fig. 4 Attached flow load distribution.

vortex-induced load distribution. Apparently, Eqs. (7) overpredict the difference between separated and attached flow load distributions, i.e., Eqs. (7) give a center of pressure too far forward. Still, the data in Fig. 3 very definitely indicate that the linear growth of vortex-induced load ceases at $\xi \le 0.4$. As a value, $\xi < 0.4$ would move the center of pressure of the vortex loads even farther forward; the deviation between predicted and measured $C_m(\alpha)$ – characteristics (Fig. 5) requires a different explanation.

It has been shown by Rainbird[21-23] that free body vortices on a sharp cone not only generate suction peaks underneath them (Fig. 6a), but that the vortices also entrain freestream air, causing higher flow shear on the leeward side than is measured at $\alpha = 0$ (Fig. 6b). Thus, instead of decreasing the "body steering effects," as for instance flare-induced separation does on a launch vehicle,[4,24,25] the leading-edge separation increases the effective apparent mass (Fig. 7).

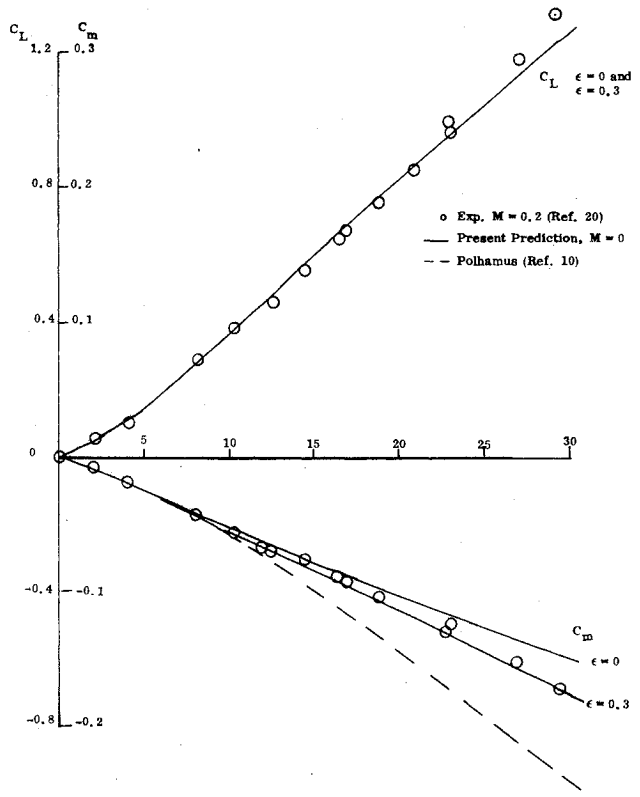

Fig. 5 Comparison between predicted and measured static characteristics of a sharp edge $A = 1.147$ delta wing.

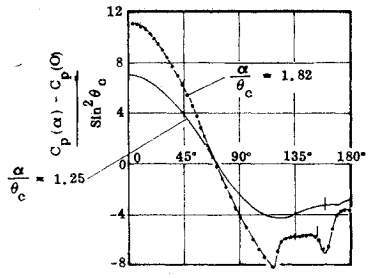

a) CIRCUMFERENTIAL PRESSURE DISTRIBUTIONS

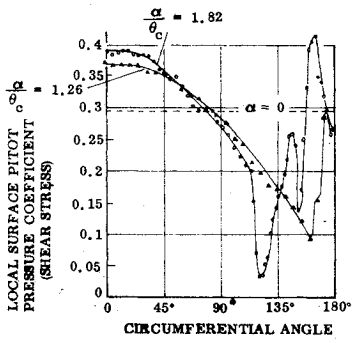

b) SURFACE SHEAR STRESS DISTRIBUTIONS AROUND CONE

Fig. 6 Free body vortex effects on a 12.5° sharp cone.[21]

Assuming that a fraction ϵ of the vortex-induced loading is caused by this increase of the attached flow-type loading, Eq. (7) is modified as

$$C_{NV} = \pi \sin^2 \alpha \tag{8a}$$

$$C_{mV} = -(c_0/\bar{c})\,\epsilon C_{NV}(\bar{\xi}_a - \xi_{CG}) - (c_0/\bar{c})\,(1-\epsilon) C_{NV}(\bar{\xi}_V - \xi_{CG}) \tag{8b}$$

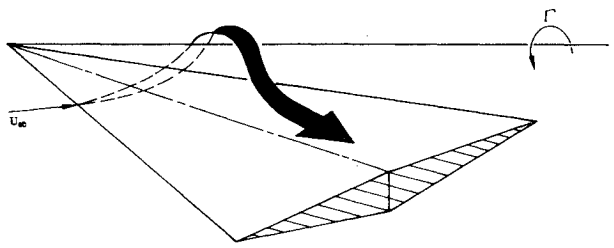

Fig. 7 Entrainment effect of leading-edge vortex.

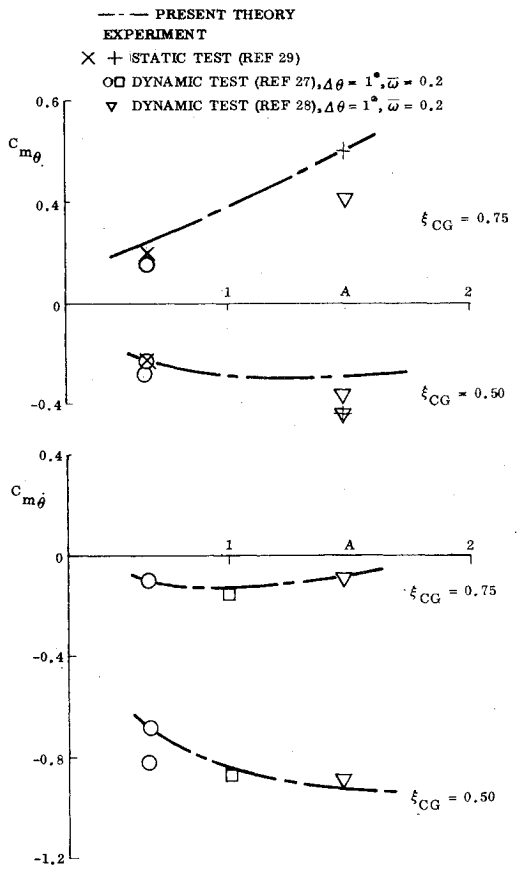

Fig. 8 Attached flow dynamic stability derivatives at $\alpha = 0$ and $M = 0$.

where $\bar{\xi}_a$ and $\bar{\xi}_V$ are defined as before, Eqs. (5) and (7).

If a value $\epsilon = 0.3$ is assumed, Eqs. (5) and (8) do predict the experimental $C_m(\alpha)$-characteristics (Fig. 5). The static characteristics determined in this manner will be used in the analysis to be performed later to determine unsteady delta wing aerodynamics. It may seem presumptuous to use experimental data for one aspect ratio, $A = 1.147$, and expect the vortex load distribution to be the same for other aspect ratios. However, it is shown in Ref. 8 that Eqs. (6) and (8) are valid also for other aspect ratios. That is, experimental data indicate that not only is the vortex-induced total lift insensitive to aspect ratio ($K_V = \pi$) but also the vortex-induced load distribution, both longitudinally and laterally, is independent of leading-edge sweep. Thus, using the $A = 1.147$ data gives good prediction also for other aspect ratios in the range of $0.65 \le A \le 1.5$.

Unsteady Aerodynamics

The unsteady aerodynamic characteristics of slender delta wings at high angles of attack are determined using the method of local linearization, i.e., by considering small perturbations from a mean static angle of attack (α_0). The total unsteady aerodynamic derivatives are then obtained by super-

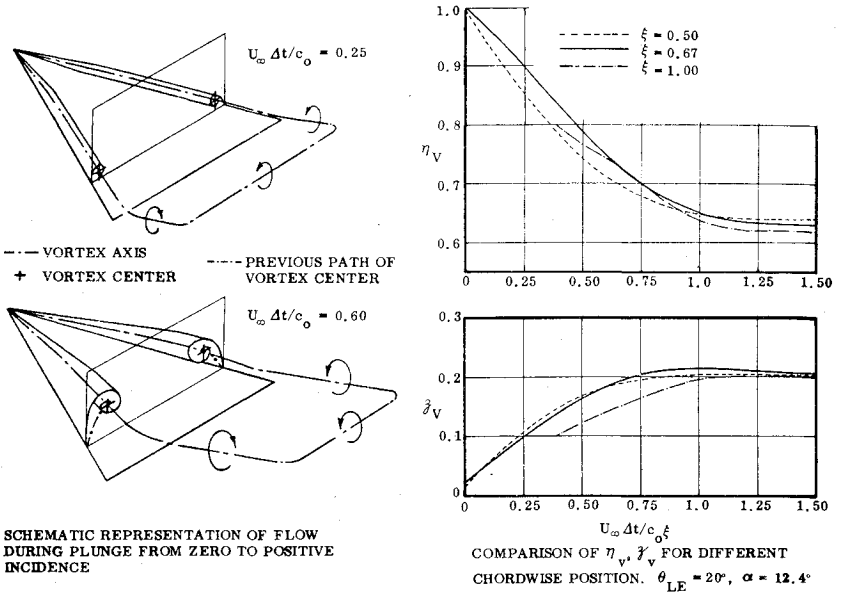

Fig. 9 Leading-edge vortex formation during plunge from zero to positive angle of attack.[32]

position of attached flow and separated flow load components.

The attached flow unsteady aerodynamic characteristics are obtained using first-order momentum theory,[26] modified to agree with Eqs. (5) in regard to static characteristics. The following equations result.[8]

$$C_{m_{\theta a}} = -(c_0/c)\ (C_{N_\alpha})_{\text{eff}} \times \cos^2\alpha_0 [(2/3)(c_{\text{eff}}/c_0) - \xi_{CG}] \tag{9a}$$

$$C_{m_{\dot\theta a}} = -(c_0/\bar c)^2 (C_{N_\alpha})_{\text{eff}} \times \cos\alpha_0 [(c_{\text{eff}}/c_0) - \xi_{CG}]^2 \tag{9b}$$

$$(C_{N_{\dot\alpha}})_{\text{eff}} = (\pi A/2)(b_{\text{eff}}/b)^2 \tag{9c}$$

$$b_{\text{eff}}/b = c_{\text{eff}}/c_0 = 0.955\cos\theta_{LE}[2 - \cos^{-2}\alpha_0]^{1/2} \tag{9d}$$

Figure 8 shows that Eqs. (9) predict the measured dynamic derivatives[27-29] at $\alpha = 0$, $M = 0$, with satisfactory accuracy up to aspect ratio $A = 1.5$. At aspect ratios above $A = 2$, the deviations probably become unacceptable and a more sophisticated approach[30] has to be used.

The separated flow unsteady aerodynamic characteristics are determined using static experimental data in an unsteady analysis, which is in large part based upon results obtained in special dynamic experiments. The transient leading-edge separation characteristics on sharp-edged delta wings have been investigated extensively by the British. Most noteworthy are the contributions made by Lambourne and his colleagues,[31-33] using a combined experimental-analytical approach. The results obtained in a water tunnel for a plunging delta wing established a very simple picture of the unsteady leading-edge separation and the formation of the leading-edge vortex (Fig. 9). The steady-state vortex position is established after a time increment $\Delta t = c_0\xi/U_\infty$. That is the vortex is convected downstream from apex with freestream speed. In the time interval before the steady-state position is reached, the transient vortex is parallel to the leading edge, as the local shedding takes place at the same rate along the leading edge. The vortex apparently reaches its steady-state height position somewhat before the time $\Delta t = c_0\xi/U_\infty$ when the steady-state spanwise position is reached.

In their most recent investigation of unsteady leading-edge vortices, Lambourne et al. studied the effect of oscillatory bending deformation of the forward half of a sharp-edged delta wing by measuring the pressure fluctuations over the rigid aft half. Distributed roughness was used over the forward 14% chord to ensure turbulent flow over the whole upper, inner surface. In the thorough "calibration" of the test setup, it was discovered that the pressure transducer housing, protruding slightly from the bottom surface, could cause a severe disturbance of the leeside vortex flow if placed near the leading edge. The result is similar to that obtained on delta wings by placement of miniscule flow fences or, rather, vortex generators on the underside of the leading edge, which cause the large continuous leading-edge vortex to break down into smaller ones. The practical consequence for Lambourne et al. was that they had to remove the outer transducer at the forward station when making measurements at the downstream, aft section. The practical consequence for the space shuttle designer could be much more far reaching.

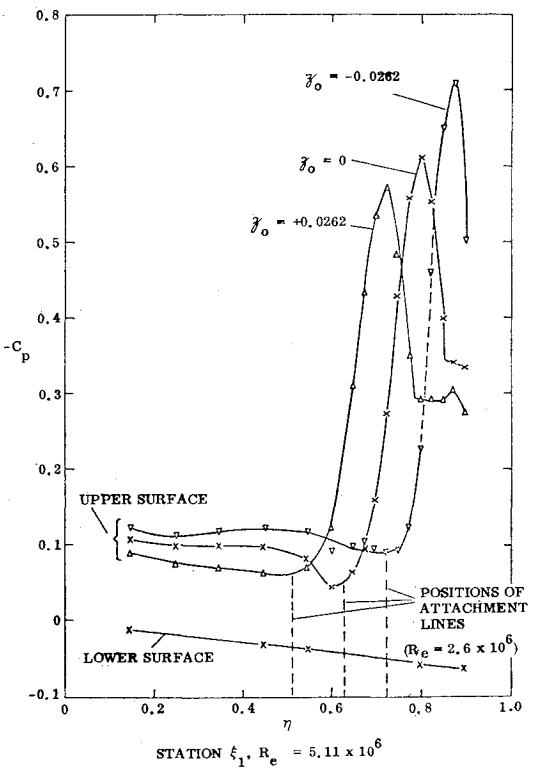

Fig. 10 Spanwise pressure distribution for steady deformation.[33]

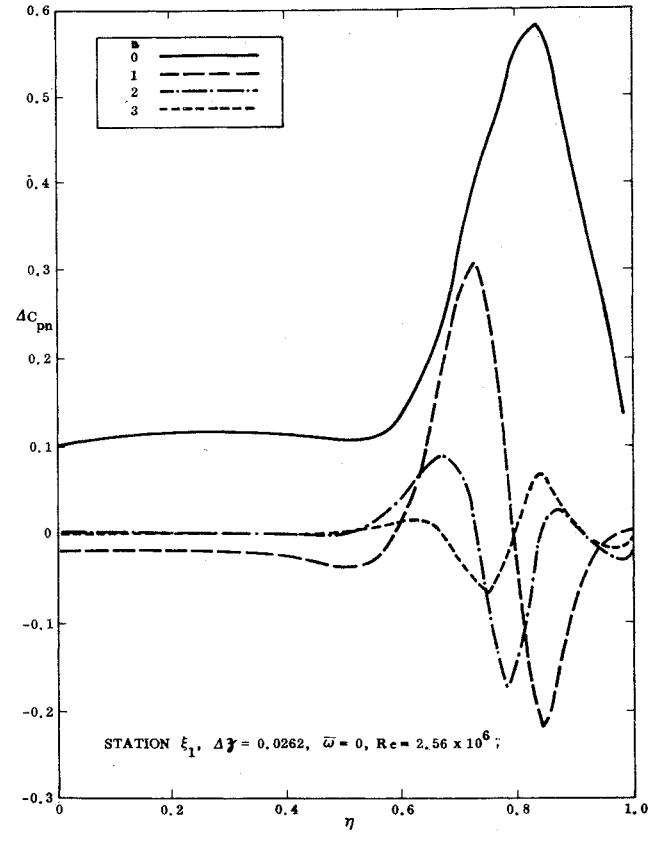

Fig. 11 Spanwise distributions of harmonic components for quasi-steady variation.[33]

The steady-state spanwise pressure distributions at maximum upward and downward deflections are compared with the undeflected wing data in Fig. 10. As expected the windward side pressures are unaffected by the wing deformation. On the leeward side the inboard pressure change caused by the deformation is explained by regular attached flow camber effects and is roughly predicted by lifting-surface theory. The outboard vortex-induced loads are affected by the deformation in a manner that is somewhat more intricate. The spanwise position of the suction peak is affected by the wing deformation in a manner consistent with the higher (α/θ_{LE})-values for the forward delta wing in the case of upward deflection,[8] causing an inboard movement of the vortex (and conversely an outboard movement for the downward deflection). Less obvious are the reasons for the changes of the suction peak magnitude in Fig. 10. Lambourne et al. suggest that the vortex movement up and away from the surface dominates over the effect of increased vortex strength for the bent-up wing, causing a loss in aft wing suction peak magnitude. An alternative or possibly complementary explanation is provided in the present analysis, i.e., the shedding sheet from the leading edge weakens earlier for the upward deflection. The reason is that α/θ_{LE} decreases along the chord, thus decelerating the vortex shedding process, whereas the opposite is true for the downward deflection. Thus, the breakdown of the vortex growth rate is reacting to longitudinal camber in the samy way as Lambourne et al. have shown vortex burst to be affected.[34] A similar α/θ_{LE}-effect is obtained by changing θ_{LE} along the chord. Thus, a Gothic wing corresponds to the positive camber (bent down apex) and should produce similar vortex-growth trends, which it indeed does[35] as discussed in detail in Ref. 8.

Figure 11 shows the effect of this quasi-steady deflection on the spanwise lift distribution. Apparently, the vortex load is not only moving in spanwise direction but is also undergoing some spanwise redistribution (or deformation). The first harmonic would be very important for a structural deformation such as wing bending (more or less parallel to the leading edge). Even the higher harmonics have some potential in this respect. This force-couple-type harmonic can make the higher wing deformation modes (with nodal lines parallel, almost, with the leading edge) critical from the standpoint of wing buffet, as is pointed out by Lambourne et al.[33]

In the oscillatory case, the distributions are very similar to those shown in Fig. 11 for the quasi-steady deformation. Lambourne et al.[33] show that the pressure variations across the span are in phase with one another, and that the phase angles increase proportionately to the order of the harmonic, i.e.,

$$\Delta\phi = K_1 n, \text{ where } K_1 = \text{constant} \tag{10}$$

They also found that the phase angle is proportional to ξ, which has also been observed on a delta wing describing plunging oscillations[36] and is, of course, in agreement with expectations based on the earlier work by Lambourne et al.[31,32]; i.e., the phase lag is determined by a constant timelag Δt.

$$\Delta\phi = n\omega\Delta t; \quad \Delta t = K_2 c_0 \xi / U_\infty \tag{11}$$

The results gave $K_2 = 1.00 \pm 0.01$, in excellent agreement with the earlier sudden-plunge results.[31,32] That the time lag would be the same for a plunging and a bending wing, i.e., independent of the chordwise (α/θ_{LE})-distribution, was demonstrated by Lambourne et al. in the following elegant manner.[33] The strength $\Gamma(\xi)$ of the vortex at any position ξ can be regarded as the integral result of the vorticity shed from all positions upstream of ξ. For conical flow $\mathrm{d}\Gamma/\mathrm{d}x$ is constant,¶ and for small perturbations can be assumed to vary linearly with the change of local angle of attack, i.e.,

$$\Delta(\mathrm{d}\Gamma/\mathrm{d}\xi) = k_1 \Delta\alpha \tag{12}$$

The perturbation of the vortex strength at any station downstream of the deformation is then given by the chordwise integral taken over the deforming part, i.e.,

$$\tilde{\Gamma}(\xi) = \Gamma(\xi,\tilde{\alpha}) - \Gamma(\xi,\alpha_0) = \int_D \frac{\mathrm{d}\Gamma}{\mathrm{d}\xi}\,\mathrm{d}\xi = k_1 \int_D \tilde{\theta}(\xi)\,\mathrm{d}\xi \tag{13}$$

In the case of static deformation $\tilde{\theta}(\xi) = \partial\zeta/\partial\xi$ and Eq. (13) gives

$$\Gamma(\xi) = -k_1 \zeta_0 \tag{14}$$

That is, the vortex-strength-perturbation is proportional to the deflection at the apex independent of the shape of the deformation. In the unsteady case, the local effective perturbation angle is

$$\tilde{\theta}(\xi) = \partial\zeta/\partial\xi + (c_0/U_\infty)\ (\partial\zeta/\partial t) \tag{15}$$

The vortex strength at a point convecting with the flow is determined by $\tilde{\theta}(\xi)$.

$$\mathrm{d}\tilde{\Gamma}(\xi)/\mathrm{d}\xi = k_1 \tilde{\theta}(\xi) \tag{16}$$

At station ξ_1, at time t_1, the vortex strength would be the sum of the vorticity shed from each position ξ upstream of ξ_1 at the earlier time $t_1 - c_0(\xi_1 - \xi)/U_\infty$. For a certain deflection $\zeta(0, t - c_0\xi_1/U_\infty)$ equal to the deflection $\zeta(0) = \zeta_0$ in the static case, the equivalent deformation shape in the unsteady case will deviate from the static deformation shape (Fig. 12a). However, because the final vortex strength $\tilde{\Gamma}(\xi)$ is independent of the deformation shape, i.e., it is insensitive to the manner $(\mathrm{d}\Gamma/\mathrm{d}\xi)$ in which the vorticity was added up-

¶ According to the discussion earlier in connection with Fig. 3, this is strictly valid only for the region close to apex, $\xi \leq 0.4$

stream of ξ_l to reach the final value, the vortex strength at ξ_l in the unsteady case is simply

$$\tilde{\Gamma}(\xi_l,t_l) = -k_l\delta(0,t_l - c_0\xi_l/U_\infty) \tag{17}$$

or with

$$\delta = \delta_0 \cos\,\omega t \tag{18a}$$

$$\tilde{\Gamma}(\xi,t) = -k_l\delta_0\cos(\omega t_l - \omega\xi_l) \tag{18b}$$

Thus, the vortex strength locally is dependent upon the apex deflection in the manner observed for the fluctuating pressure in the experiment. Lambourne et al. conclude that although the pressure variations are very dependent upon the height- and span-wise movements of the vortex, these movements are probably themselves dependent upon the changes in vortex strength, and Eq. (18) would apply also for the pressure variations. Thus, the pressure variations are in the unsteady case simply determined by phase lagging the quasi-steady pressure variations. That is, the pressure amplitude is not modulated by the frequency. This constant-time-lag, constant-amplitude solution is exactly what the present authors have used as the low frequency approximation of the Karman-Sears vortex-wake effects in two-dimensional airfoil flow.[37,38]

In regard to the cautionary remarks by Lambourne et al. that their derivation considers only convection of disturbances that are upstream of the observation point, (and neglects pressure changes caused by disturbances downstream of the observation point), the following observation can be made. The local vortex strength will determine the local pressures as long as the reduced frequency is low because then the "neighborhood" vortex-strength-deviations from this local value, upstream and downstream from the observation point, are negligibly small. That is, the derived results for the pressure variation are valid only for low frequencies. When the frequency is high, this "lumped-timelag" approximation is no longer good.

The sketches in Fig. 12 illustrate why plunging and bending oscillations have the same timelag. A series of quasi-steady rigid wings make up the forward vortex-shedding body in the case of plunging oscillations, but the equivalent deformation concept still holds, as long as the vortex follows the local wing flow, which is already implied in the conic-flow-assumption. For the same reason, the effect of the forward wing deformation on downstream vortex-induced pressures will be the same, regardless of whether or not the aft wing is rigid or is also describing some sort of unsteady deformation.** That is, the present authors believe the results obtained by Lambourne et al. to have a wider application than they have assumed. Mathematically, the vortex-induced load component†† has the same form as the forced induced by a flow separation spike (the spike tip corresponding to the apex[4]).

$$C_{m\dot{\theta}s} = C_{m\dot{\theta}s1} + C_{m\dot{\theta}s2} \tag{19a}$$

$$C_{m\dot{\theta}s} = C_{m\dot{\theta}s1} + C_{m\dot{\theta}s2} \tag{19b}$$

$$C_{m\dot{\theta}s1} = -(c_0/\bar{c})\,\epsilon\, C_{N\alpha V}(\bar{\xi}_a - \xi_{CG}) \tag{19c}$$

$$C_{m\dot{\theta}s2} = -(c_0/\bar{c})\;(1-\epsilon)C_{N\alpha V}(\bar{\xi}_V - \xi_{CG}) \tag{19d}$$

$$C_{m\dot{\theta}s1} = -(c_0/\bar{c})^2\epsilon C_{N\alpha V} \times \sec\alpha_0[(c_{\rm eff}/c_0) - \xi_{CG}]^2 \tag{19e}$$

$$C_{m\dot{\theta}s2} = -(c_0/\bar{c})\,\xi_{CG}\,(U_\infty/\bar{U})\;C_{m\dot{\theta}s2} \tag{19f}$$

where $\bar{\xi}_a$ and $\bar{\xi}_v$ are obtained from Eqs. (5) and (7), $c_{\rm eff}/c_0$ from Eqs. (9), and $C_{N\alpha V}$ from Eqs. (7).

**The $\xi \le 0.4$ restriction for the conic flow assumption imposes the same error in both cases.

††Exclusive of entrainment effects, i.e., $(1-\epsilon)C_{NV}$ in Eq. (8).

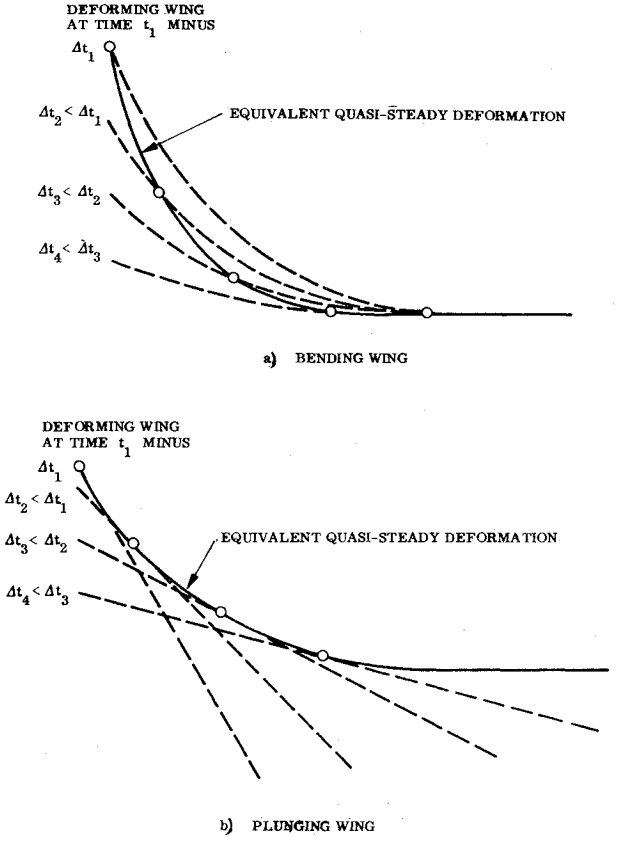

Fig. 12 Deformation shapes for vortex build-up in steady and unsteady case.

In the plunging test performed by Lambourne et al.,[32] it was observed that the leading-edge vortex reached its steady-state height position before it reached the steady-state spanwise position (Fig. 9). Thus, it is suggested by the vortex-height data that a value of $U_\infty/\bar{U} = 0.75$ should be used when computing the pitch damping. In the case of the vortex-induced rolling moment, $U_\infty/\bar{U} = 1.00$ would, of course, be the representative value. The fact that the pressure oscillations for the deforming wing[33] gave $U_\infty/\bar{U} = 1.00$ does not contradict the previous conclusion. As the pressure measurements gave meaningful phase lag results only in the region of the vortex-induced suction peak (over the center region of the wing the harmonic response amplitudes were insignificant), where the pressure changes registered by a fixed pressure transducer will be very sensitive to the spanwise vortex movement, the pressure data should give $U_\infty/\bar{U} = 1.00$. Finally, the implication $\bar{U} > U_\infty$ is completely in accord with measured velocities in the vortex core.[39,40]

Figure 13 shows that the predictions through Eqs. (9) and (19), with $\epsilon = 0.3$ and $U_\infty/\bar{U} = 0.75$, agree rather well with dynamic experimental data[27,28] for $A = 0.654$ and $A = 1.484$ delta wings (Figs. 13a and 13b, respectively). Consequently, one can with a high degree of confidence apply the present formulation of unsteady attached flow and vortex-induced loads to determine the aeroelastic characteristics of the space shuttle lift-off configuration including the effects of delta wing leading-edge separation. While other complications exist in the case of the space shuttle delta wing caused by rounded leading-edge effects, control-induced flow separations, flow interference effects from parallel, and main booster tanks with rocket exhaust plumes,[8,41] the results obtained for sharp-edged delta wings are very encouraging and promise that analysis techniques developed earlier for Apollo-Saturn launch vehicles[4,24,25] can be extended to include the effects of large lifting surfaces such as the orbiter delta wing. How this could be done is outlined in some detail in Ref. 8.

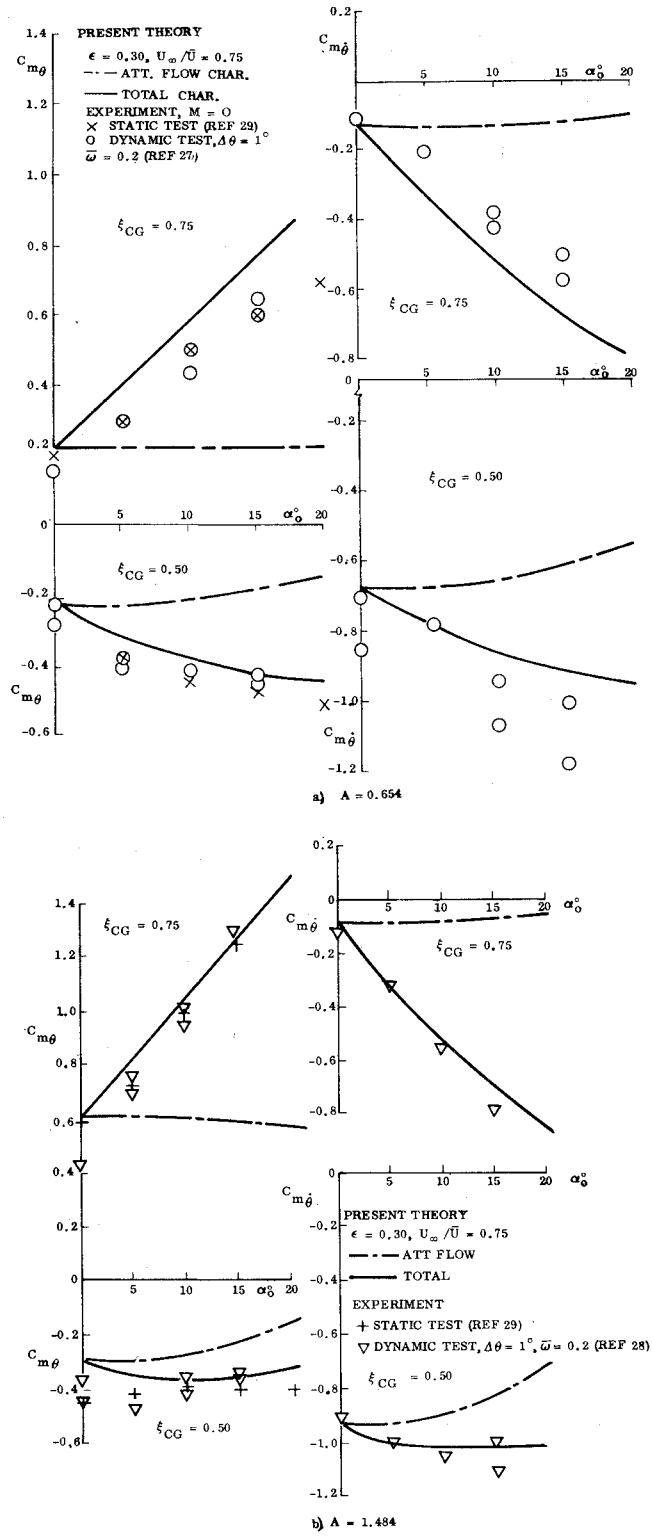

Fig. 13 Dynamic stability derivatives for sharp-edged delta wings at $M=0$.

Conclusions

A study of steady and unsteady aerodynamics of sharp-edged slender delta wings has shown the following: 1) Through a simple modification Jones' slender wing theory can give the potential flow static loads in incompressible flow. 2) A redistribution of Polhamus' vortex lift, based upon experimental data and postulated vortex entrainment effects, provides accurate prediction of delta wing aerodynamic center at high angles of attack. 3) The attached flow delta wing, unsteady aerodynamics are obtained using first-order momentum theory applied to an equivalent slender wing defined such that it gives agreement with potential flow theory in regard to static loads. Damping derivatives computed in this manner for incompressible flow at $\alpha=0$ agree well with experimental results for aspect ratios up to $A=1.5$. 4) The effects of leading-edge vortices on slender wing unsteady aerodynamics are obtained using vortex-induced loads defined by use of static experimental data in an unsteady analysis based upon Lambourne's simple convective timelag concept. The dynamic derivatives determined in this manner over a large angle-of-attack range agree well with available experimental data.

References

[1] Runyan, H. L. and Reed, W. H., "Dynamics and Aeroelasticity—An Appraisal," *Astronautics & Aeronautics*, Vol. 9, Feb. 1971, pp. 48-57.

[2] Tischler, A. O., "Critical Areas—Thermal-Protection Systems, Vehicle Weights, and—Aeroelasticity," *Astronautics & Aeronautics*, Vol. 9, Aug. 1971, p. 8.

[3] Ericsson, L. E. and Reding, J. P., "Report on Saturn I-Apollo Unsteady Aerodynamics," LMSCA650215, Contract NAS 8-5338, Feb. 1964, Lockheed Missile & Space Co., Sunnyvale, Calif.

[4] Ericsson, L. E. and Reding, J. P., "Analysis of Flow Separation Effects on the Dynamics of a Large Space Booster," *Journal of Spacecraft and Rockets*, Vol. 2, July-Aug. 1965, pp. 481-490.

[5] Rainey, A. G., "Progress on the Launch Vehicle Buffeting Problem," *Journal of Spacecraft and Rockets*, Vol. 2, May-June 1965, pp. 289-299.

[6] Ericsson, L. E. and Reding, J. P., "Technical Summary Report, Aeroelastic Characteristics of Saturn 1B and Saturn V Launch Vehicles," LMSC M-37-67-5, Contract NAS 8-11238, Dec. 1967, Lockheed Missiles & Space Co., Sunnyvale, Calif.

[7] Hanson, P.W. and Doggett, R.V. Jr., "Aerodynamic Damping and Buffet Response of an Aeroelastic Model of the Saturn I Block II Launch Vehicle," TN D-2713, March 1965, NASA.

[8] Ericsson, L. E. and Reding, J. P., "Unsteady Aerodynamic Analysis of Space Shuttle Vehicles," LMSC D352320, Contract NAS 8-28130, Aug. 1973, Lockheed Missiles & Space Co., Sunnyvale, Calif.

[9] Polhamus, E. C., "A Concept of the Vortex Lift of Sharp-Edge Delta Wings Based on a Leading-Edge-Suction Analogy," TN D-3767, Dec. 1966, NASA.

[10] Polhamus, E. C., "Predictions of Vortex-Lift Characteristics by a Leading-Edge-Suction Analogy," *Journal of Aircraft*, Vol. 8, April 1971, pp. 193-199.

[11] Jones, R. T., "Properties of Low-Aspect-Ratio Pointed Wings at Speeds Below and Above the Speed of Sound," Rept. 835, May 1945, NASA.

[12] Hummel, D., "Zur Umströmung scharfkantiger schlanker Deltaflügel bei grossen Anstellwinkeln," *Zeitschrift fuer Flugwiss*, Vol. 15, Oct. 1967, pp. 376-385.

[13] Smith, J. H. B., "Improved Calculations of Leading-Edge Separation from Slender Delta Wings," RAE Tech. Rept. 66070, March 1966, Aeronautical Research Council, London.

[14] Örnberg, T., "A Note on the Flow Around Delta Wings," KTH Aero TN 38, Feb. 1954, Royal Institute of Technology, Stockholm, Sweden.

[15] Wentz, W. H. Jr., "Effects of Leading-Edge Camber on Low-Speed Characteristics of Slender Delta Wings," CR-2002, Oct. 1972, NASA.

[16] Snyder, M. H. Jr. and Lamar, J. E., "Appliction of the Leading-Edge Suction Analogy to Prediction of Longitudinal Load Distribution and Pitching Moments for Sharp-Edged Delta Wings," TND-6994, Aug. 1972, NASA.

[17] Margason, R. J. and Lamar, J. E., "Vortex-Lattice FORTRAN Program for Estimating Subsonic Aerodynamic Characteristics of Complex Planforms," TN D-6142, Feb. 1971, NASA.

[18] Maltby, R. L. Engler, P. B., and Keating, R. F. A., with Addendum by Moss, G. F., "Some Exploratory Measurements of Leading-Edge Vortex Postions on a Delta Wing Oscillating in Heave," R&M 3176, July 1963, Aeronautical Research Council, London.

[19] Elle, B. J., "An Investigation at Low Speed of the Flow Near the Apex of Thin Delta Wings with Sharp Leading Edges," R&M 3176, Jan. 1958, Aeronautical Research Council, London.

[20] Davenport, E. E. and Huffman, J. K., "Experimental and Analytical Investigation of Subsonic Longitudinal and Lateral

Aerodynamic Characteristics of Slender Sharp-Edge 74° Swept Wings," TND-6344, July 1971, NASA.

[21] Rainbird, W. J., "Turbulent Boundary-Layer Growth and Separation on a Yawed Cone," *AIAA Journal*, Vol. 6, Dec. 1968, pp. 2410-2516.

[22] Rainbird, W. J., Crabbe, R. S., and Jurewics, L. S., "A Water Tunnel Investigation of the Flow Separation About Circular Cones at Incidence," Aero. Rept. LR-385, Sept. 1963, National Research Council, National Aeronautical Establishment, Ottawa, Canada.

[23] Rainbird, W. J., "The External Flow Field about Yawed Circular Cones at Incidence," *AGARD Conference Proceedings No. 30*, May 1968, pp. 19-1-19-20.

[24] Ericsson, L. E., Reding, J. P., and Guenther, R. A., "Launch Vehicle Gust Penetration Loads," *Journal of Spacecraft and Rockets*, Vol. 9, Jan. 1972, pp. 19-25.

[25] Ericsson, L. E., Reding, J. P., and Guenther, R. A., "Elastic Launch Vehicle Response to Sinusoidal Gusts," *Journal of Spacecraft and Rockets*, Vol. 10, April 1973, pp. 244-252.

[26] Bisplinghoff, R. L., Ashley, J., and Halfman, R. L., *Aeroelasticity*, Addison-Wesley, Cambridge, Mass. 1955, pp. 418-419.

[27] Woodgate, L., "Measurements of the Oscillatory Pitching Moment Derivatives on a Slender Sharp-Edged Delat Wing in Incompressible flow," R&M No. 3628, Part 2, July 1968, Aeronautical Research Council, London.

[28] Woodgate, L. and Pugh, P. G., "Measurements of the Pitching-Moment Derivatives on a Sharp-Edged Delta Wing in Incompressible Flow," R&M No. 3379, Oct. 1963, Aeronautical Research Council, London.

[29] Woodgate, L. and Halliday, A. S., "Measurements of Lift, Drag, and Pitching Moments on a Series of Three Delta Wings," R&M No. 3628, Part 4, July 1968, Aeronautical Research Council, London.

[30] Woodcock, D. L., "A Comparison of Methods Used in Lifting Surface Theory," AGARD Rept. 583, June 1971.

[31] Lambourne, N. C., Bryer, D. W., and Maybrey, J. F. M., "A Preliminary Note on the Behavior of the Leading-Edge Vortices on a Delta Wing Following a Sudden Change of Incidence," NPL Aero Note 1006, Nov. 1962, Aeronautical Research Council, London.

[32] Lambourne, N. C., Bryer, D. W., and Maybrey, J. F. M., "The Behavior of the Leading-Edge Vortices over a Delta Wing Following a Sudden Change of Incidence," R&M No. 3645, March 1969, Aeronautical Research Council, London.

[33] Lambourne, N. C., Bryer, D. W., and Maybrey, J. F. M., "Pressure Measurements on a Model Delta Wing Undergoing Oscillatory Deformation," NPL Aero Report 1314, March 1970, Aeronautical Research Council, London,

[34] Lambourne, N. C. and Bryer, D. W., "The Bursting of Leading-Edge Vortices—Some Observations and Discussion of the Phenomenon," R&M No. 3282, April 1961, Aeronautical Research Council, London.

[35] Peckham, O. H., "Low-Speed Wind-Tunnel Tests on a Series of Uncambered Slender Pointed Wings with Sharp Edges," R&M 3186, Dec. 1958, Aeronautical Research Council, London.

[36] Keating, R. F. A., "Measurement of Pressures on a Delta Wing Oscillating in Heave at a High Angle of Incidence," RAE Rept. 67241, Oct. 1967, Aeronautical Research Council, London.

[37] von Karman, Th. and Sears, W. R., "Airfoil theory for Non-Uniform Motion," *Journal of Aeronautical Science*, Vol. 5, Aug. 1938, pp. 379-390.

[38] Ericsson, L. E. and Reding, J. P., "Unsteady Airfoil Stall, Review and Extension," *Journal of Aircraft*, Vol. 8, Aug. 1971, pp. 609-616.

[39] Earnshaw, P. B., "An Experimental Investigation of a Leading Edge Vortex," R&M No. 3281, March 1961, Aeronautical Research Council, London.

[40] Lambourne, N.C. and Bryer, D.W., "Some Measurements in the Vortex Flow Generated by a Sharp Leading Edge Having 65° Sweep," CP 477, July 1959, Aeronautical Research Council, London.

[41] Reding, J. P. and Ericsson, L. E., "Unsteady Aerodynamics Could Dominate the Space Shuttle Booster Aeroelastic Stability," AIAA Paper 74-362, Las Vegas, Nev., 1974.